

COMMONSENSE KNOWLEDGE ASSISTED DEEP LEARNING WITH APPLICATION TO SIZE-RELATED FINE-GRAINED OBJECT DETECTION

Pu Zhang, Bin Liu*

Research Center for Applied Mathematics and Machine Intelligence, Zhejiang Lab
Hangzhou 311121, China

ABSTRACT

In this paper, we focus on a scenario where a single image contains objects of the same category but varying sizes, and we propose a lightweight approach that can not only recognize their category labels but also their real sizes. Our approach utilizes commonsense knowledge to assist a deep neural network (DNN) based coarse-grained object detector to achieve accurate size-related fine-grained detection. Specifically, we introduce a commonsense knowledge inference module (CKIM) that maps the coarse-grained labels produced by the DL detector to size-related fine-grained labels. Experimental results demonstrate that our approach achieves accurate fine-grained detections with a reduced amount of annotated data, and smaller model size, compared with baseline methods. Our code is available at: <https://github.com/ZJLAB-AMMI/CKIM>.

Index Terms— deep learning, commonsense knowledge, object detection, fine-grained detection

1. INTRODUCTION

In this paper, we consider size-related fine-grained object detection. This problem appears in many real-life scenarios. For example, imagine we ask a robot to fetch a cup for us. In the robot’s field of view, there are cups of various sizes, but we want the robot to grab the cup of an expected size accurately. Therefore, the robot not only needs to recognize the presence of cups in the scene but also detect the size of each cup to achieve the desired task. In autonomous driving, there are also times when we want the algorithm to automatically detect people as well as their size-related attributes, so that it can discriminate adults and children, as the driving strategies for adults and children are likely to be different.

Modern deep learning (DL) based methods, such as YOLO [1] and Faster R-CNN [2], have become the dominant approach to object detection as it significantly improves detection accuracy. However, the benefits of these advancements come at a cost: the requirement on substantial computational and storage resources, along with a vast quantity of annotated data. This challenge is further compounded in the fine-grained

case of our concern, which demands even larger models, more annotated data, and greater computational budgets to train and store the model [3].

In this paper, we propose a lightweight deep neural network (DNN)-based detector for fine-grained objects that are size-related. When presented with a test image containing multiple objects of the same category but varying in size, our approach can efficiently determine the category and size of each object. The core idea is to leverage commonsense knowledge, independent of specific tasks, to enhance the performance of a coarse-grained object detector. To achieve this, we identify two valuable pieces of commonsense knowledge and introduce a commonsense knowledge-based inference module (CKIM) that collaborates with the coarse-grained object detector. The CKIM can infer fine-grained object labels based on the output generated by the coarse-grained detector. Fig. 1 illustrates the distinctions between traditional fine-grained detectors and our proposed approach.

2. RELATED WORKS

2.1. Modern DNNs for Visual Object Detection

There are two major types of modern DNN based object detectors. One is termed two-stage detectors, such as Faster R-CNN [2], which include networks with separate modules for candidate region generation and classification. The second type is single-stage detectors, which directly produce object categories and their bounding boxes in a single step and use predefined differently sized boxes to locate objects. Single-stage detectors are suitable for real-time, resource-constrained scenarios such as edge computing because they have lightweight designs and require less time to make predictions. So we employ them as benchmark object detectors in this paper.

You Only Look Once (YOLO) is one of the most widely used single-stage object detectors [4]. In YOLO, the input image is divided into a grid with $S \times S$ cells, and each cell predicts bounding boxes and their corresponding class probabilities. Over time, newer versions of YOLO, such as YOLOv4 [5] and YOLOv7, have been proposed to improve inference speed and reduce model size. Both YOLOv4 and YOLOv7 have lightweight versions, namely YOLOv4-tiny and YOLOv7-tiny,

* Address correspondence to bins@ieee.org. This work was supported by Exploratory Research Project (No.2022RC0AN02) of Zhejiang Lab.

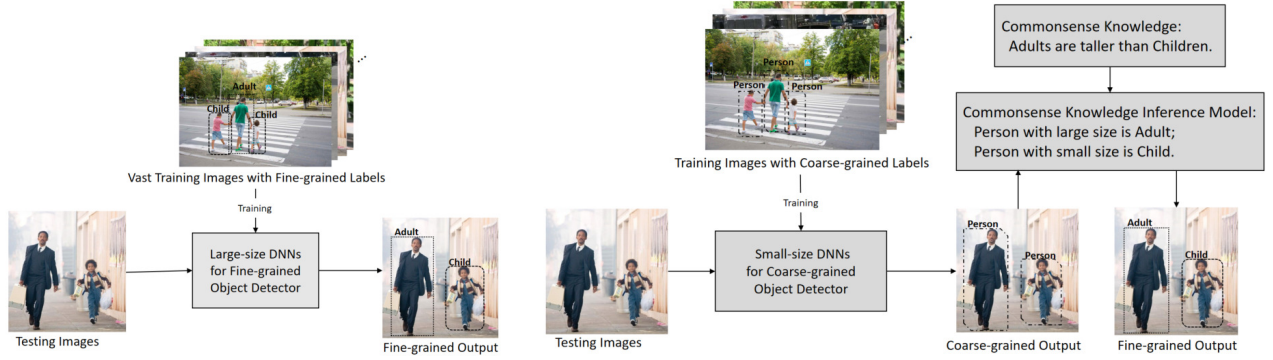


Fig. 1: Comparison of the working mechanisms between a typical fine-grained object detector (left) and our approach (right)

which employ smaller model architectures that are better suited for edge computing scenarios [6, 7]. In our experiments, we use YOLOv7-tiny as a baseline method.

MobileNet-SSD is an efficient DL method for object detection in mobile computing scenarios. It employs a Single Shot MultiBox Detector (SSD) [8] as the decoder and MobileNet [9] as the feature extractor. SSD was the first single-stage detector that performed comparably to two-stage detectors. MobileNet was specifically designed for vision applications on mobile devices, with traditional convolution layers replaced by depthwise separable and pointwise convolution layers to reduce model size [10]. An advanced version of MobileNet, MobileNetV3, uses a search algorithm to optimize the network architecture [11]. In our experiments, we use MobileNetV3-SSD as a baseline method.

2.2. Neural-Symbolic Approaches

Neural-symbolic approaches aim to integrate the complementary strengths of machine learning and symbolic reasoning [12, 13, 14]. There are different ways to combine DL and symbolic knowledge. One approach involves translating symbolic knowledge into continuous vector representations and treating them as inputs for DL models [15, 16]. Another approach is to instruct the training process of DL models with symbolic knowledge, such as by embedding the knowledge into the loss function [17]. Finally, it is also possible to perform symbolic reasoning based on the outputs of DL algorithms [18, 19].

Our approach falls into the category of performing symbolic reasoning based on the outputs of DL algorithms. However, it differs from other methods in this category in several ways. Firstly, our target task is different. Secondly, the knowledge we employ is distinct from what has been used in prior neural-symbolic approaches. In particular, we identify and utilize two specific pieces of commonsense knowledge that are unique to our approach. Lastly, we develop novel techniques to effectively combine our knowledge with the outputs of modern coarse-grained object detectors.

3. OUR APPROACH

In this section, we present our approach for size-related fine-grained object detection. As shown in the right panel of Fig. 1, our approach consists of two parts: a coarse-grained object detector and CKIM. The former part outputs coarse-grained labels and a bounding box for each object. The bounding box can be represented by:

$$\text{box}(C, X, Y, W, H) \quad (1)$$

where C denotes the coarse-grained label, (X, Y) denotes the coordinates of the centre of the bounding box, and W and H denote the width and height of the bounding box, respectively. We focus on size-related fine-grained labels in this work. The real size of an object is naturally closely related to the size of the object’s bounding box, which can be produced by a qualified object detector. In addition, according to commonsense knowledge as follows

Knowledge 1 *An object appears to decrease in size as it moves farther away and appears to enlarge as it moves closer to the observer;*

the real size of an object is related to its distance from the camera. For an object in an image, we can estimate its real distance to the camera based on its distance from the center of its bounding box to the bottom of the image. This is because:

Knowledge 2 *the object’s distance to the camera (D_{toC}) is strongly connected to the distance from the center of its bounding box to the bottom of the image (C_{toB}).*

The connection between C_{toB} to D_{toC} is illustrated in Fig. 2.

We validated the accuracy of the aforementioned two pieces of commonsense knowledge on a diverse range of datasets. The results in Table 1 demonstrate that **Knowledge 1** consistently holds true. Moreover, **Knowledge 2** is confirmed to be valid on all three autonomous driving datasets considered, with a probability exceeding 98% for life scene image datasets, and with a probability surpassing 95% for two indoor

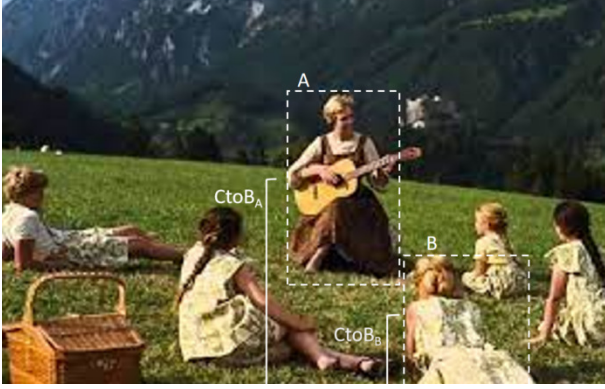


Fig. 2: An example image that illustrates the connection between an object’s distance to the camera (DtoC) and the distance from the center of the object to the bottom of the image (CtoB). As shown in the image, CtoB of object A, denoted by $CtoB_A$, is larger than $CtoB_B$. This information can be used to infer that DtoC of object A, denoted by $DtoC_A$, is larger than $DtoC_B$, which is clearly true as shown in the picture.

robot-related datasets. However, **Knowledge 2** does not hold for two remote sensing image datasets since they are captured using top-down satellite imagery. See more info. in Sec.7.5.

Datasets		Knowledge 1	Knowledge 2
Autonomous Driving	BDD 100K	100%	100%
	CityPersons	100%	100%
	KITTI	100%	100%
Indoor	Habitat AI	100%	95%
Robots	OpenLORIS	100%	96%
Remote Sensing	WHU-RS19	100%	0%
	RSSCN7	100%	0%
Life Scenes	MSCOCO	100%	99%
	LVIS	100%	98%
	PASCAL VOC	100%	99%

Table 1: The validity of these two commonsense knowledge on 10 benchmark datasets

The aforementioned commonsense knowledge provides us with an opportunity to reason size-related fine-grained labels from the outputs of a coarse-grained object detector, such as the coarse-grained labels and bounding boxes of the objects. The purpose of CKIM is to infer fine-grained labels based on the size of the objects’ bounding boxes (BoxS) and their distances to the camera (DtoC). To achieve this, we normalize values of X , Y , W , H according to the width and height of the image, define the size of the bounding box (BoxS) as its area, and define DtoC as 1 minus Y . Then, we calculate BoxS and DtoC as follows:

$$\begin{aligned} BoxS &= W \times H \\ DtoC &= 1 - Y \end{aligned} \quad (2)$$

Next, we construct a classifier, namely the CKIM, represented as $f(x)$, where $x \triangleq (BoxS, DtoC)$. This classifier maps the input x to size-related attributes of the object: ‘large’, ‘middle’, or ‘small’. Since x comprises only two dimensions, this classifier is relatively small in terms of model size and requires fewer labeled data for training compared to fine-grained DNN models. In our experiments, we considered two types of classifiers, implemented using crisp-rule and fuzzy-rule approaches, respectively. Further details can be found in Sec.7.1.

One may question how to acquire commonsense knowledge. Frequently, it is derived from the experience or intuition of human experts. Alternatively, it can also be obtained from a large language model, as preliminarily explored by us in Sec.7.6.

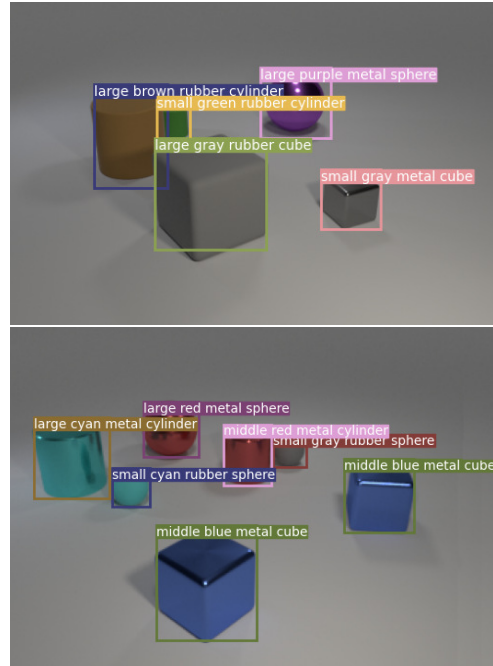


Fig. 3: Top: an example image in the CLEVR-96 dataset, where the object size attribute is specified as either ‘large’ or ‘small’; Bottom: an example image in the CLEVR-144 dataset, where the object size attribute can be ‘large’, ‘middle’, or ‘small’.

4. EXPERIMENTS

We experimentally evaluated the performance of our proposed CKIM-assisted DNN detector. We compared our method against the SOTA methods, including YOLOv7-tiny and MobileNetv3-SSD, both being developed for resource-constrained scenarios. We integrated CKIM with YOLOv7-tiny and MobileNetv3-SSD and assessed whether it resulted in improved performance.

4.1. Experimental Setup

We conducted experiments on the open-source CLEVR data set [20]. It consists of images containing objects and questions related to them. The objects’ attributes include size (big, small), color (brown, blue, cyan, gray, green, purple, red, yellow), material (metal, rubber), and shape (cube, cylinder, sphere). According to these attributes, objects are divided into 96 fine-grained categories. We term this dataset as CLEVR-96. In our experiment, when using our approach, we removed the size attribute to train a lightweight object detector that considers $96/2 = 48$ coarse-grained labels at first. Then, for each test image, our approach employs this lightweight object detector to yield category label for it, then invoke the CKIM to infer its size attribute, namely the fine-grained label. To simulate complex environments in the real world, we constructed a new dataset by introducing a collection of objects of middle size. It has 144 fine-grained classes. We term this dataset as CLEVR-144 in what follows. See Fig.3 for example pictures in these datasets. Both CLEVR-96 and CLEVR-144 contain 16,000 images as the training set, 2,000 images as the validation set, and the other 2,000 images as the test set.

4.2. Performance Metrics

In our evaluation, we considered three different perspectives: detection accuracy, model size, and processing latency:

- Detection Accuracy is measured by the mean Average Precision while $\text{IoU}=0.5$ ($\text{mAP}@0.5$), which is a commonly used metric for evaluating object detectors. It calculates the mean of the average precision over all classifications for every bounding box with an IoU greater than 0.5. Larger $\text{mAP}@0.5$ means higher accuracy.
- Model Size is measured by the memory space that the model consumes. This is important in resource-constrained scenarios where memory is limited.
- Latency is defined as the average time a method takes to process one image. In our experiments, the time unit was set as millisecond (ms). This is also an important factor to consider in resource-constrained scenarios where real-time processing is required.

4.3. Experimental Results

We trained all the involved models using all 16,000 images in the training set. The performance of these models on the CLEVR-96 and CLEVR-144 datasets are shown in Tables 2 and 3, respectively. We observe that our approach outperforms both baseline methods in terms of Detection Accuracy, Model Size and Latency. Since this dataset only has two fine-grained labels (‘small’ and ‘large’), there is no label ambiguity issue involved. So only the crisp-rule based version of our approach is considered in the experiment. On the CLEVR-144 dataset,

	Accuracy \uparrow	Model Size \downarrow	Latency \downarrow
MobileNetv3_SSD	0.968	87.61MB	82
Our approach	0.978	49.63MB+2KB	60
YOLOv7-tiny	0.972	23.31MB	70
Our approach	0.983	22.89MB+2KB	62

Table 2: Experiments on the CLEVR-96 dataset. The best performances for each model type are highlighted in **bold**. In contrast to the fine-grained object detector (MobileNetv3 or YOLOv7-tiny) trained with all 96 fine-grained labels, our approach utilizes a much lighter version of MobileNetv3 or YOLOv7-tiny. This lightweight model is trained with only 48 coarse-grained labels by excluding the size attribute from the dataset. The size-related fine-grained labels of the test images are inferred using the CKIM component of our approach.

	Accuracy \uparrow	Model Size \downarrow	Latency \downarrow
MobileNetv3_SSD	0.970	125.59MB	84
Our approach(crisp)	0.968	49.63MB+2KB	61
Our approach(fuzzy)	0.978	49.63MB+2KB	62
YOLOv7-tiny	0.965	23.73MB	75
Our approach(crisp)	0.971	22.89MB+2KB	64
Our approach(fuzzy)	0.980	22.89MB+2KB	62

Table 3: Experiments on the CLEVR-144 dataset

which involves three fine-grained labels (‘small’, ‘middle’, and ‘large’), Table 3 shows that the fuzzy-rule based version of our approach is preferable to the crisp-rule based one. This demonstrates the ability of the fuzzy method to deal with semantic ambiguity in the fine-grained labels.

We also evaluated a baseline fine-grained YOLOv4 model. On the CLEVR-96 dataset, this model achieves a high detection accuracy of 0.998, but has a much larger model size of 246.35MB and latency of 176ms than the methods listed in Table 2. On the CLEVR-144 dataset, it achieves detection accuracy of 0.998 again, while it also has a much larger model size of 247.34MB and latency of 183ms than the methods listed in Table 3.

5. CONCLUSIONS

In this paper, we focused on a particular fine-grained object detection problem: efficiently identifying the category of each object and determining its size in images containing multiple objects of the same category but varying in sizes. Unlike typical fine-grained object detectors that rely on fine-grained data annotations, our approach does not require such detailed annotations. Furthermore, we demonstrated that our approach is lightweight, faster, and more computationally efficient compared to conventional fine-grained detectors, while maintaining higher detection accuracy.

6. REFERENCES

- [1] J. Redmon and A. Farhadi, “Yolov3: An incremental improvement,” *arXiv preprint arXiv:1804.02767*, 2015. 1
- [2] S. Ren, K. He, R. Girshick, and J. Sun, “Faster R-CNN: Towards real-time object detection with region proposal networks,” *Advances in Neural Information Processing Systems*, vol. 28, 2015. 1
- [3] S. Zaidi, M. Ansari, A. Aslam, N. Kanwal, M. Asghar, and B. Lee, “A survey of modern deep learning based object detection models,” *Digital Signal Processing*, p. 103514, 2022. 1
- [4] J. Redmon, S. Divvala, R. Girshick, and A. Farhadi, “You only look once: Unified, real-time object detection,” in *Proc. of the IEEE/CVF Conf. on Computer Vision and Pattern Recognition*, 2016, pp. 779–788. 1
- [5] A. Bochkovskiy, C. Wang, and H. M. Liao, “Yolov4: Optimal speed and accuracy of object detection,” *arXiv preprint arXiv:2004.10934*, 2020. 1
- [6] C. Wang, A. Bochkovskiy, and H. M. Liao, “Scaled-yolov4: Scaling cross stage partial network,” in *Proc. of the IEEE/CVF Conf. on Computer Vision and Pattern Recognition*, 2021, pp. 13029–13038. 2
- [7] C. Wang, A. Bochkovskiy, and H. M. Liao, “Yolov7: Trainable bag-of-freebies sets new state-of-the-art for real-time object detectors,” *arXiv preprint arXiv:2207.02696*, 2022. 2
- [8] W. Liu, D. Anguelov, D. Erhan, C. Szegedy, S. Reed, C. Fu, and A. C. Berg, “SSD: Single shot multibox detector,” in *Proc. of European Conf. on Computer Vision*, 2016, pp. 21–37. 2
- [9] A. G. Howard, M. Zhu, B. Chen, D. Kalenichenko, W. Wang, T. Weyand, M. Andreetto, and H. Adam, “Mobilenets: Efficient convolutional neural networks for mobile vision applications,” *arXiv preprint arXiv:1704.04861*, 2017. 2
- [10] M. Sandler, A. Howard, M. Zhu, A. Zhmoginov, and L. Chen, “Mobilenetv2: Inverted residuals and linear bottlenecks,” in *Proc. of the IEEE/CVF Conf. on Computer Vision and Pattern Recognition*, 2018, pp. 4510–4520. 2
- [11] A. Howard, M. Sandler, G. Chu, L. Chen, B. Chen, M. Tan, W. Wang, Y. Zhu, R. Pang, and V. Vasudevan, “Searching for mobilenetv3,” in *Proc. of the IEEE/CVF Inter. Conf. on Computer Vision*, 2019, pp. 1314–1324. 2
- [12] K. Yang, *Neurosymbolic Machine Learning for Reasoning*, Ph.D. thesis, Princeton University, 2022. 2
- [13] A. Garcez, S. Bader, H. Bowman, L. C. Lamb, L. de Penning, B. Illuminoo, H. Poon, and C. G. Zaverucha, “Neural-symbolic learning and reasoning: A survey and interpretation,” *Neuro-Symbolic Artificial Intelligence: The State of the Art*, vol. 342, no. 1, pp. 327, 2022. 2
- [14] D. Yu, B. Yang, D. Liu, H. Wang, and S. Pan, “A survey on neural-symbolic learning systems,” *Neural Networks*, 2023. 2
- [15] T. Mikolov, I. Sutskever, K. Chen, G. S. Corrado, and J. Dean, “Distributed representations of words and phrases and their compositionality,” *Advances in Neural Information Processing Systems*, vol. 26, 2013. 2
- [16] J. Pennington, R. Socher, and C. D. Manning, “Glove: Global vectors for word representation,” in *Proc. of Conf. on Empirical Methods in Natural Language Processing (EMNLP)*, 2014, pp. 1532–1543. 2
- [17] M. Nickel, L. Rosasco, and T. Poggio, “Holographic embeddings of knowledge graphs,” in *Proc. of the AAAI Conf. on artificial intelligence*, 2016, vol. 30. 2
- [18] K. Yi, J. Wu, C. Gan, A. Torralba, P. Kohli, and J. Tenenbaum, “Neural-symbolic vqa: Disentangling reasoning from vision and language understanding,” *Advances in neural information processing systems*, vol. 31, 2018. 2
- [19] T. Eiter, N. Higuera, J. Oetsch, and M. Pritz, “A neuro-symbolic asp pipeline for visual question answering,” *Theory and Practice of Logic Programming*, vol. 22, no. 5, pp. 739–754, 2022. 2
- [20] J. Johnson, B. Hariharan, L. Van Der Maaten, L. Fei-Fei, C. Lawrence Zitnick, and R. Girshick, “CLEVR: A diagnostic dataset for compositional language and elementary visual reasoning,” in *Proc. of the IEEE Conf. on Computer Vision and Pattern Recognition*, 2017, pp. 2901–2910. 4
- [21] Michael P LaValley, “Logistic regression,” *Circulation*, vol. 117, no. 18, pp. 2395–2399, 2008. 6
- [22] Fangyi Li, Changjing Shang, Ying Li, Jing Yang, and Qiang Shen, “Approximate reasoning with fuzzy rule interpolation: background and recent advances,” *Artificial Intelligence Review*, vol. 54, no. 6, pp. 4543–4590, 2021. 6
- [23] V Kreinovich, Ch Quintana, and L Reznik, “Gaussian membership functions are most adequate in representing uncertainty in measurements,” in *Proceedings of NAFIPS*, 1992, vol. 92, pp. 15–17. 6
- [24] Rafał Scherer, *Multiple fuzzy classification systems*, vol. 288, Springer, 2012. 6

7. APPENDIX

7.1. CKIM Assisted Object Detection

In this section, we explain how to specify CKIM using commonsense knowledge and how to use it to assist a coarse-grained deep detector in doing fine-grained object detection. We develop two types of CKIM, corresponding to crisp-rule and fuzzy-rule based inference.

7.1.1. Crisp-rule based CKIM

In crisp rule-based systems, Boolean logic is followed, and an object can only belong to one class or not belong to it. We model the relationship between the real size of an object and its attributes given by a coarse-grained object detector using a logistic regression function [21].

To simplify the presentation, we consider size-related object labels: ‘large’, ‘middle’, and ‘small’. We use the one-vs-rest method to perform crisp rule inference. The decision function of the crisp rule is defined as follows:

$$\begin{aligned} f_{ml}(BoxS, DtoC) &= \frac{1}{1 + e^{w_{ml}^T x}}, x \triangleq (BoxS, DtoC) \\ f_{sm}(BoxS, DtoC) &= \frac{1}{1 + e^{w_{sm}^T x}}, \end{aligned} \quad (3)$$

where f_{sm} denotes the decision function for small sized and middle sized objects, and f_{ml} the decision function for middle sized and large sized objects, w^T is a set of parameters optimized by minimizing a cost function in the same way as in typical logistic regression.

Accordingly, the CKIM is defined as follows:

If $f_{ml}(BoxS, DtoC) > 0$,
then the object’s fine-grained label is ‘large’;
If $f_{ml}(BoxS, DtoC) < 0$ and $f_{sm}(BoxS, DtoC) > 0$,
then the fine-grained label is ‘middle’;
If $f_{sm}(BoxS, DtoC) < 0$,
then the fine-grained label is ‘small’.

7.1.2. Fuzzy-rule based CKIM

In real-life cases, there may be continuous-valued attributes (e.g., size, distance, age) that are difficult to classify with discrete semantic descriptions (e.g., large or small, near or far, young or old), resulting in semantic vagueness or uncertainty. Fuzzy logic provides a multi-value logic, in which such vague semantics can be strictly formulated and precisely studied.

To adapt our method to more general scenarios, we propose a fuzzy-rule based approach for implementing CKIM. Fuzzy rule-based systems allow an object to match different categories with different memberships. We adopt the aforementioned Mamdani model for this task, which uses fuzzy sets as rule antecedents and consequents. Two main categories of

membership functions are typically used in constructing fuzzy sets [22]:

(1) Polygonal functions, such as triangular shaped and trapezoidal shaped functions;

(2) Nonlinear functions, including Gaussian shaped and generalised bell shaped functions.

Here, we adopt the Gaussian-shaped membership function [23]. As before, we consider size-related object labels, namely ‘large’, ‘middle’, and ‘small’.

In our fuzzy rule inference module, the antecedents of rules are defined as follows:

$$\begin{aligned} M_L(x) &= \mathcal{N}(x|\mu_L, \Sigma_L) \\ &= \frac{1}{2\pi|\Sigma_L|^{1/2}} \exp \left\{ -\frac{1}{2} (x - \mu_L)' \Sigma_L^{-1} (x - \mu_L) \right\} \\ M_M(x) &= \mathcal{N}(x|\mu_M, \Sigma_M) \\ &= \frac{1}{2\pi|\Sigma_M|^{1/2}} \exp \left\{ -\frac{1}{2} (x - \mu_M)' \Sigma_M^{-1} (x - \mu_M) \right\} \\ M_S(x) &= \mathcal{N}(x|\mu_S, \Sigma_S) \\ &= \frac{1}{2\pi|\Sigma_S|^{1/2}} \exp \left\{ -\frac{1}{2} (x - \mu_S)' \Sigma_S^{-1} (x - \mu_S) \right\} \end{aligned} \quad (4)$$

where $x \triangleq (BoxS, DtoC)$ the same as before; S , M and L in the subscripts denote ‘small’, ‘middle’, and ‘large’, respectively; μ and Σ denote the mean and covariance matrix of the data distribution.

The fuzzy-rule based CKIM is designed as follows:

If x matches M_L , then object’s label is ‘large’ with degree $M_L(x)$;

If x matches M_M , then object’s label is ‘middle’ with degree $M_M(x)$;

If x matches M_S , then object’s label is ‘small’ with degree $M_S(x)$.

A crisp output is then calculated by a defuzzification approach to integrate membership degrees between the object and all rules. Accordingly, the fine-grained result is determined by the arg max function defined as follows:

$$Label = \arg \max_{i \in \{S, M, L\}} M_i(x) \quad (5)$$

Note that since these two types of CKIM have few parameters to be optimized, the amount of data required to train them is almost negligible compared to those required to train a DNN model.

7.2. An example show of a fuzzy inference process using a Mamdani model

Mamdani models [24] are widely used in FRBS. They use fuzzy sets as rule antecedents and consequents, as shown in Fig. 4, and perform inference by integrating the conclusions of individual rules that overlap with the input. The weight of a certain rule is determined by the match degree between the input instance and the rule antecedent.

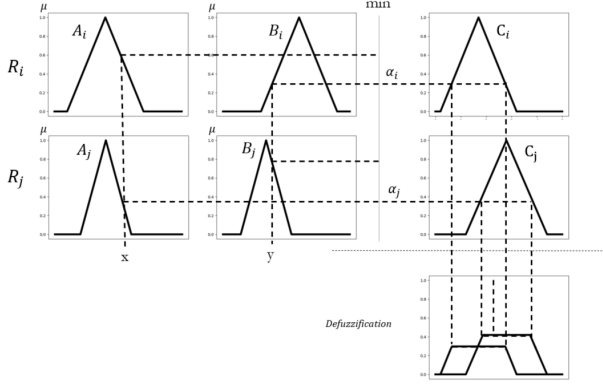


Fig. 4: Illustrative example of the inference process with a Mamdani model. R_i, R_j represent two fuzzy rules; $(A_i, B_i), (A_j, B_j)$ are the corresponding antecedents for the rules R_i, R_j respectively; C_i, C_j are their consequent for fuzzy rule R_i, R_j respectively; (x, y) is the input instance; α_i, α_j stand for matching degrees between the input and the two rules.

7.3. On experiments with 5,000 randomly selected images being used for model training

In order to simulate cases where the edge device does not have enough memory space to store all training data, we conducted experiments using 5,000 randomly selected images from the training set for model training. The experimental results on the CLEVR-96 and CLEVR-144 datasets are presented in Tables 4 and 5, respectively.

As shown in the tables, for the case with less training data, the benefits given by our proposed method become more remarkable. Our method outperforms all baseline methods according to all performance metrics. In addition, we once again observed the benefits of fuzzy inference on the CLEVR-144 dataset. The fuzzy-based method significantly outperforms the crisp-rule based method in terms of detection accuracy.

	Accuracy \uparrow	Model Size \downarrow	Latency \downarrow
MobileNetv3_SSD	0.902	87.61MB	82
Our Approach	0.912	49.63MB+2KB	60
YOLOv7-tiny	0.928	23.31MB	71
Our Approach	0.984	22.89MB+2KB	61

Table 4: Fine-grained object detection performance on the CLEVR-96 dataset using 5,000 randomly selected images for model training. All terms are defined in the same way as in Table 2. As part of our experiment, we also evaluated a baseline fine-grained YOLOv4 model. This model achieves a high detection accuracy of 0.972, but has a much larger model size of 246.35MB and latency of 178ms than the methods listed here.

	Accuracy \uparrow	Model Size \downarrow	Latency \downarrow
MobileNetv3_SSD	0.857	125.59MB	83
Our Approach (crisp)	0.862	49.63MB+2KB	60
Our Approach (fuzzy)	0.877	49.63MB+2KB	59
YOLOv7-tiny	0.865	23.73MB	72
Our Approach (crisp)	0.892	22.89MB+2KB	65
Our Approach (fuzzy)	0.914	22.89MB+2KB	62

Table 5: Fine-grained object detection performance on the CLEVR-144 dataset using 5,000 randomly selected images for model training. As part of our experiment, we also evaluated a baseline fine-grained YOLOv4 model. This model achieves a high detection accuracy of 0.957, but has a much larger model size of 247.34MB and latency of 175ms than the methods listed here.

7.4. Training process comparison for fine-grained and coarse-grained object detectors

In order to investigate the difference in the training process between fine-grained and coarse-grained object detectors, we conducted an experiment using the YOLOv7-tiny model. Specifically, we compared the training process of a YOLOv7-tiny based fine-grained detector and a YOLOv7-tiny based coarse-grained detector. The results, shown in Fig. 5, demonstrate that the coarse-grained detector converges much faster than its fine-grained counterpart on both the CLEVR-96 and CLEVR-144 datasets.

Since our proposed fine-grained object detector consists of a coarse-grained detector and a lightweight CKIM, the convergence speed of our method is almost the same as the coarse-grained detector it employs. This indicates that the convergence speed of our proposed fine-grained detector is much faster than its counterpart fine-grained detector.

Overall, these results demonstrate that our proposed method achieves efficient and effective fine-grained object detection by leveraging a lightweight commonsense knowledge inference module with a coarse-grained object detector, achieving high accuracy while maintaining fast convergence times.

7.5. On the Validity of Our Selected Commonsense Knowledge

To test the validity of the two commonsense-knowledge, we conducted an brief investigation on 10 popular benchmark datasets in 4 scenarios: autonomous driving, indoor robots, life scenes, and remote sensing. Specifically, we randomly selected 500 images which contain size-related categories, such as children and adults, car and bus, football and tennis fields, and check whether the two pieces of commonsense-knowledge are valid. The results of our investigation is summarized in Table 1. It turns out that Knowledge 1 consistently holds true. Moreover, Knowledge 2 is confirmed to be valid on all three

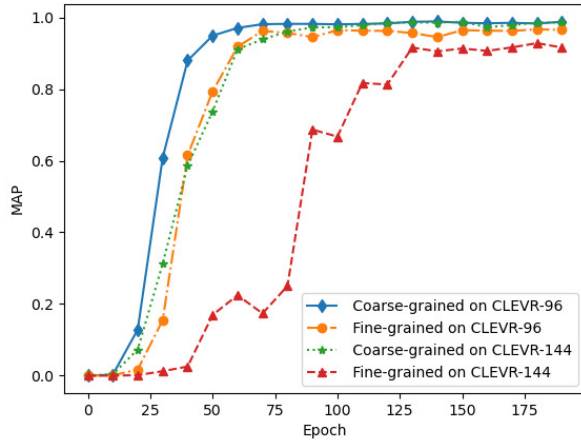


Fig. 5: Training process of a pair of fine-grained and coarse-grained object detectors

autonomous driving datasets considered, with a probability exceeding 98% for life scene image datasets, and with a probability surpassing 95% for two indoor robot-related datasets. However, Knowledge 2 does not hold for two remote sensing image datasets. We found that Knowledge 2 is not valid when

- The camera position for photographing the objects is located directly above or directly below the objects, as shown in Fig.7;
- The objects in the picture are located on different horizontal planes, as shown in Fig.8.

7.6. On the Potential of using large language models (LLMs) to Generate Commonsense Knowledge

To explore the potential of using LLMs to generate commonsense knowledge, we conducted several prompt designs utilizing the Vicuna-7B model, a commonly used open-source LLM model. The response of the LLM can be observed in Fig. 9. The results demonstrate that LLMs are indeed capable of generating significant commonsense knowledge.

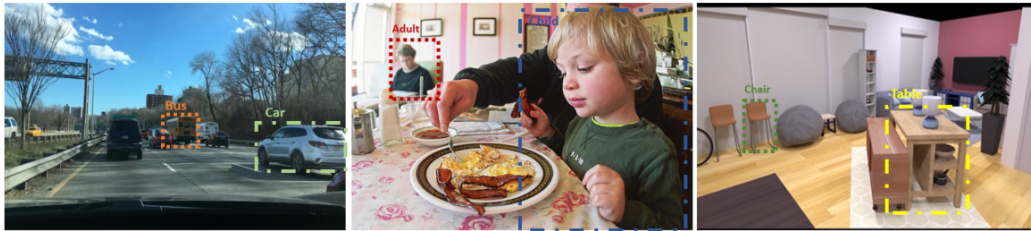


Fig. 6: Example images for which the two pieces of commonsense-knowledge are valid. Left: autonomous driving; Middle: life scenes; Right: indoor robots



Fig. 7: Examples images for which the camera position for photographing the objects is located directly above or directly below the objects. Left: image of flying birds; Right: remote sensing images



Fig. 8: Example images in which the objects are located on different horizontal planes. Left: a baby lifted in the air; Middle: teenagers jumping in the air; Right: Bowl in the cupboard and cup on the counter.

Prefix Prompt

Instruction:

You are an information provider for distinguish fine-grained objects according to coarse-grained objects in object detection task.

Interaction

Question: How to distinguish **adults** and **children** from **person** label?

LLM Response: You can try the following approaches:

1. Height estimation: adults are taller than children.
2. Proportions: children tend to have different body proportions compared to adults.
3. Contextual information: leveraging contextual cues present in the image.
4. Data augmentation: training a model on other datasets with adults and children.

Question: Only the information of bounding box is available

LLM Response: There are a few possibilities that you can explore:

1. **Bounding box size:** children generally have smaller body proportions compared to adults.
2. **Body proportions:** within the bounding box: head of children appears larger compared to the rest of the body.

Question: How to distinguish **cars** and **buses** from **vehicle** label?

LLM Response: You can try the following approaches:

1. Data augmentation: collect images of cars and buses from other sources.
2. Pre-trained model: using models pretrained on dataset with cars and buses.
3. Post-processing techniques: applying post-processing techniques to refine your results., such as size or aspect ratio of the detected bounding boxes.

Question: Only the information of bounding box is available

LLM Response: There are a few possibilities that you can explore:

1. **Aspect ratio:** buses have a higher aspect ratio compared to cars.
2. **Size:** Buses are generally larger than cars.

Fig. 9: Example shows of prompt designs for an LLM that automatically provides knowledge to help distinguish between fine-grained and coarse-grained labels. The prefix prompt offers task instructions, and during the interaction with LLM, only fine-grained and coarse-grained labels need to be provided. Moreover, the attributes used for distinguishing fine-grained labels can be generated automatically.